Journal of Atmospheric and Solar-Terrestrial Physics 73 (2011) 1166–1172

Contents lists available at ScienceDirect

Journal of Atmospheric and Solar-Terrestrial Physics

journal homepage: www.elsevier.com/locate/jastp

On 3D reconstruction of coronal mass ejections: II. Longitudinal and latitudinal width analysis of 31 August 2007 event

M. Mierla [a,b,c,*], B. Inhester [d], L. Rodriguez [b], S. Gissot [b], A. Zhukov [b,e], N. Srivastava [f]

[a] Institute of Geodynamics of the Romanian Academy, Jean-Louis Calderon 19-21, Bucharest-37, RO-020032, Romania
[b] Solar-Terrestrial Center of Excellence SIDC, Royal Observatory of Belgium, Belgium
[c] Research Center for Atomic Physics and Astrophysics, Faculty of Physics, University of Bucharest, Romania
[d] Max-Planck Institute for Solar System Research, Germany
[e] Skobeltsyn Institute of Nuclear Physics, Moscow State University, Moscow, Russia
[f] Udaipur Solar Observatory, Physical Research Laboratory, Udaipur, India

ARTICLE INFO

Article history:
Received 31 March 2010
Received in revised form
22 November 2010
Accepted 24 November 2010
Available online 2 December 2010

Keywords:
Coronal mass ejections
Reconstruction
STEREO

ABSTRACT

In an earlier work, Mierla et al. (2009) applied four different reconstruction techniques to three coronal mass ejections (CMEs) at a given time. This study is a follow up of the above work in which we apply a local correlation tracking and tie-point reconstruction technique (LCT–TP) to the CME observed on 31 August 2007 by the COR1 and COR2 coronagraphs onboard the STEREO spacecraft at different times. The results show considerable scatter in the direction parallel to the line of sight, which is a direct indication of the CME depth. We derive the longitudinal and latitudinal sizes of the CME as a function of time. We find that a reasonable lower estimate of the longitudinal size is 18°–44° with an absolute largest extent of 78°–110°. We also find that a reasonable lower estimate for the latitudinal size of the CME is 18°–32° with an absolute largest extent of 44°–56°. In general, the latitudinal size is smaller than the longitudinal size, indicating an elliptical cone like structure or a flux rope like structure with very little tilt relative to the ecliptic. Self-similar expansion is observed above a height of $6.9R_{\odot}$. As our analysis is based on a statistical approach, large scatter is expected. In order for the method to be validated, more cases have to be studied.

1. Introduction

Coronal mass ejections (CMEs) are very energetic solar phenomena which can affect us directly by the geomagnetic disturbances produced when they interact with the Earth's magnetosphere (e.g. Srivastava and Venkatakrishnan, 2004; Gopalswamy et al., 2007). It is, therefore, important to be able to derive the kinematics and three-dimensional (3D) configuration of CMEs right from their initiation, in order to accurately predict their arrival time to the Earth and their possible impact on geospace.

Since the launch of the STEREO spacecraft in October 2006, several reconstruction techniques have been successfully used to derive the direction of propagation and true speed of CMEs at distances close to the Sun (see Mierla et al., 2010 for review of techniques within the coronagraph field of view) and in the interplanetary space (see Rouillard, this issue; Howard, this issue; Jackson et al., this issue for reviews of techniques within the HI and SMEI fields of view). However, inferring their full 3D geometry from only two vantage points is still a task difficult to achieve. One complication comes from the fact that the CME plasma is optically thin and its observed radiance results from the integration of the photospheric scattered light by the coronal electrons along the line of sight. In addition, the Thomson scattering introduces a weighting factor that maximizes the radiation scattered from the electrons located close to the plane of the sky (e.g. Billings, 1966; Vourlidas and Howard, 2006; Howard and Tappin, 2009). This introduces a bias for CME intensities that are detected by a coronagraph.

Reconstruction of the full 3D geometric shape have been attempted for several CMEs by using forward modeling (e.g. Thernisien et al., 2009), and by using the polarized ratio method based on Thomson scattering geometry (e.g. Moran and Davila, 2004; Dere et al., 2005; Moran et al., 2010). Different approaches to derive the 3D geometry are given in Antunes et al. (2009) and Wood et al. (2009). Antunes et al. (2009) used forward modeling in combination with inversion method in order to reconstruct the 3D mass distribution of a CME, while Wood et al. (2009) used an intuitive trial-and-error method, where synthetic SECCHI images were computed from an assumed 3D density distribution, and then the distribution was iteratively altered until the best visual agreement with the data were obtained. Each of these approaches

* Corresponding author at: Institute of Geodynamics of the Romanian Academy, Jean-Louis Calderon 19-21, Bucharest-37, RO-020032, Romania.
E-mail addresses: marilena@geodin.ro, mmierla@gmail.com (M. Mierla).

1364-6826/$ - see front matter © 2010 Elsevier Ltd. All rights reserved.
doi:10.1016/j.jastp.2010.11.028

have their limitations. In the forward modeling method, it is necessary to assume a CME shape function that depends on several parameters; in the polarized ratio method, only the weighted mean distance of the CME density from the plane of sky can be derived. The inverse modeling is constrained by the limits on the overlapping viewpoints and in general produces non-unique solutions if only a few view directions are provided.

In this paper, we make an attempt to reconstruct the 3D geometry of a CME observed on 31 August 2007 at the south-west limb of the Sun by SECCHI-COR1 and -COR2 coronagraphs onboard STEREO. We used the local correlation tracking plus tie-pointing method (LCT–TP). The method has an advantage as it does not suffer from the constraints of the methods mentioned above, but it has its own limitations as discussed in Section 4. This paper is a follow-up work of a previous research (Mierla et al., 2009) where four different reconstruction techniques were applied to the CME images at a given time. We extend the study by applying LCT–TP method to the CME at different times.

The paper is structured as follows: Section 2 deals with the data presentation and the general description of the CME on 31 August 2007. Section 3 presents the method and its application to the data. In Section 4 the results of the 3D reconstruction are presented. The main constraints in deriving the 3D reconstruction of the CME are also presented and discussed. The main results and conclusions are summarized in the last section.

2. Description of the CME on 31 August 2007

The CME on 31 August 2007 was observed as a "three-part" CME as defined by Illing and Hundhausen (1986), in white-light, by SECCHI-COR1 and -COR2 coronagraphs onboard STEREO. The separation angle between the STEREO spacecraft on that day was approximately 28°. The CME was associated with an eruptive prominence that was observed in ultraviolet (304 Å) by SECCHI-EUVI, at around 19:00 UT. The erupting plasma is seen as a filament in EUVI-A images, and as a limb prominence in EUVI-B images (A stands for the STEREO spacecraft moving ahead of the Earth and B for the spacecraft moving behind the Earth). The filament has a U-shape, oriented almost parallel to the solar limb. The prominence material is later seen as the core of a structured CME in COR1 field of view (around 20:50 UT—COR1-A and 20:55 UT—COR1-B) and COR2 FOV (around 21:52 UT—COR2-A, and 22:23 UT—COR2-B). The cadence of images is 5 min for COR1 and 30 min for COR2 polarization sequences. Only paired images were considered for the present analysis. In this study, the total brightness images of COR1 and COR2 were used. The images were derived from three sequential images taken with polarization angle of 0°, 120° and 240°, by means of SolarSoft routine secchi_prep. In order to remove the intensity contribution of coronal streamers and visualize the intensity contribution of the CME we subtract a minimum intensity image. This image is obtained by computing the minimum value in each pixel, from a set of images ranging over a period of several hours, centered on the CME time.

Fig. 1 shows the eruption in EUVI 304, COR1 and COR2 images at specific instants. Left panels represent the images recorded by STEREO-B and right panels the ones recorded by STEREO-A. COR1 and COR2 images were rotated to align them with the STEREO mission plane (SMP), where SMP is defined as the plane which contains the two spacecraft A and B and the center of the Sun. As a consequence, we roll the images such that the SMP north corresponds to the *Y*-axis in the image. The images from STEREO-B are brought to the same Sun center and the same resolution as the STEREO-A images. To reduce the calculation time, we exclude all parts of the images not covered by the CME by selecting a region of interest (ROI). We choose it manually by marking the points on the boundary of the ROI. All the calculations are done only for the pixels which lie within the ROI.

3. The LCT–TP method and its application to the data

We apply the LCT–TP (local correlation tracking plus tie-point reconstruction) method in order to reconstruct the 3D geometry of the CME. The method is described in Mierla et al. (2009). It consists in identifying the same feature appearing in the two A and B images with the help of LCT method, and then, by using triangulation, determine the position of the feature in 3D. The projections of a feature will lie along corresponding epipolar lines (Inhester, 2006) (also known as epipolar constraint), which reduces our search to a one-dimensional search. As part of the preprocessing steps, we rectified the images such that epipolar lines are orientated horizontally in the image, and as a consequence, the correlation between normalized intensities is calculated along horizontal lines. We choose a search window of 256×3 pixels, the correlation coefficient being calculated for each pixel of this window within a match window of 11×11 pixels, centered on the pixel; 11 pixels correspond to approximately $0.08R_{\odot}$ (56 000 km) for COR1 and $0.3R_{\odot}$ (209 000 km) for COR2. In order to find correlations, we keep the match window in a fixed position on a given epipolar line in one image and move it along the same epipolar line in the other image (or in the search window). When a maximum of the correlation occurs at a certain shift, the center position of the "window" is used for tie-pointing the 3D region which has produced this high correlation. The shift, known also as disparity, is directly proportional to the reconstructed depth. The depth is defined as the distance of a feature from the plane of the sky of a virtual observer half way between the two spacecraft. The size of our search window restricts the reconstruction of the CME to a depth range of $\pm 2R_{\odot}$ for COR1 and $\pm 8R_{\odot}$ for COR2. The values of the correlation coefficients range between -1 (anticorrelation) and 1 (maximum correlation). For the present study, we have ignored all the points where the correlation coefficients were smaller than 0.9.

Fig. 2 shows the reconstructed CME at around 21:30 UT (COR1—upper panels) and at around 01:52 UT (COR2—lower panels). The Sun is represented by the gray sphere. The radius of the outer gridded sphere is $1.5R_{\odot}$. The colors represent the distance along the *X*-axis (blue indicating maximum positive value). The coordinate system used here is Heliocentric Earth Equatorial (HEEQ) coordinate system. It has its origin at the center of the Sun, the *Z*-coordinate axis along the solar rotation axis and the *X*-axis so that Earth lies in the *X*–*Z* plane. The *Y*-axis is perpendicular to the *X*- and *Z*-axes and points towards the western limb of the Sun. Two viewpoints are chosen for presenting the reconstructions: head-on in the right panel (*X* and *Z* in the image plane, *Z* downwards and *X* towards right) and edge-on in the left panel (*Y* and *Z* in the image plane, *Z* upwards and *Y* towards right). The images show some scatter along the line of sight (approximately in *X* direction), best seen from the head-on perspective. Also, notice that the CME propagates roughly in the *Y* direction.

4. Analysis of the reconstructed CME

4.1. Results

We have applied the method described in Section 3 to the COR1 images taken in the time interval 21:05–22:10 UT, and to COR2 images recorded between 22:52 UT (31 August 2007) and 04:52 UT (1 September 2007).

Fig. 3 shows the histograms of points versus longitude (upper panels) and latitude (lower panels) for the CME observed at

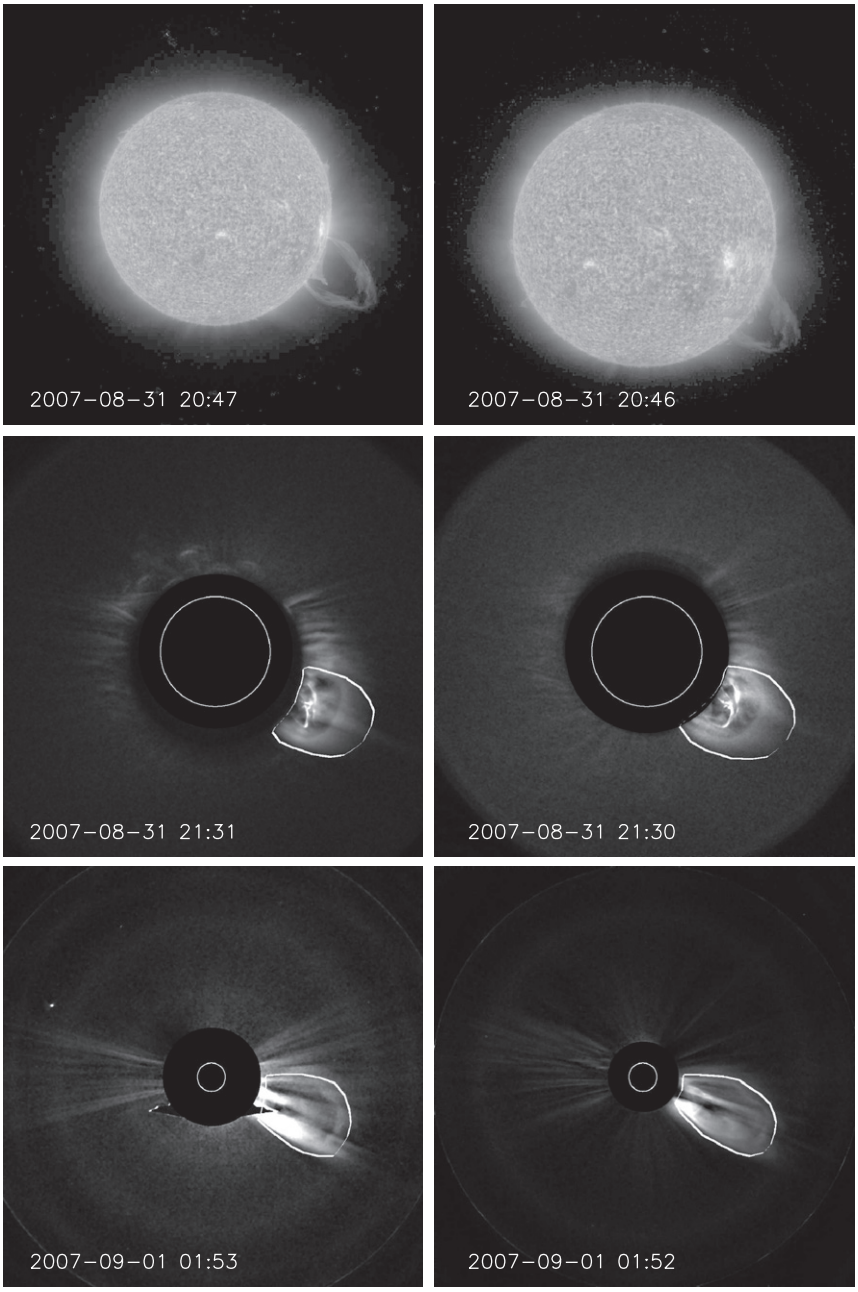

Fig. 1. CMEs on 31 August 2007, as observed by EUVI (upper panel images), COR1 (middle panel images) and COR2 (lower panel images). Right column shows images from STEREO-A, and left column, images from STEREO-B. The ROI is encircled by the white curve.

21:30 UT in COR1 field of view (left panels), and at 01:52 UT in COR2 field of view (right panels). The vertical dotted lines indicate the width and the vertical dashed lines indicate the extent of the CME. Two peaks of the distribution are observed in the upper left panel of Fig. 3, which may represent two different structures inside the CME. One of the structures may be the CME core, well separated from the rest. This is not observed in COR2 images (upper right panel of Fig. 3). The longitudinal extent, defined as $Lon_{max} - Lon_{min}$, where Lon_{max} and Lon_{min} represent the maximum and the minimum values of the longitude of the reconstructed CME (upper panels) shows a larger range compared with its latitudinal extent $Lat_{max} - Lat_{min}$, but at the same time the points are more clustered for longitude as compared with the latitude. This indicates the fact that the derivation of the longitude is more prone to errors as compared with its latitude. This is expected, as the derivation of the distance along line-of-sight has been shown to be more prone to larger reconstruction errors (see e.g. Inhester, 2006).

As our analysis is based on a statistical approach, large scatter is expected. We define the width of the distribution in longitude/latitude (or longitudinal/latitudinal width) as $2 \cdot \sigma$ and analyze its behavior in time. Note the difference between the two terms introduced: longitudinal (latitudinal) width and longitudinal (latitudinal) extent. The longitudinal width is a lower reasonable estimate for the physical size of the CME in the east–west direction, whereas the longitudinal extent is the absolute largest size of the CME in the east–west direction. Similar comments would apply for the latitudinal width and extent, except these dimensions are in the north–south direction.

In Fig. 4 we plot the mean values of the reconstructed points, indicating CME direction of propagation, and the $2 \cdot \sigma$ width of the

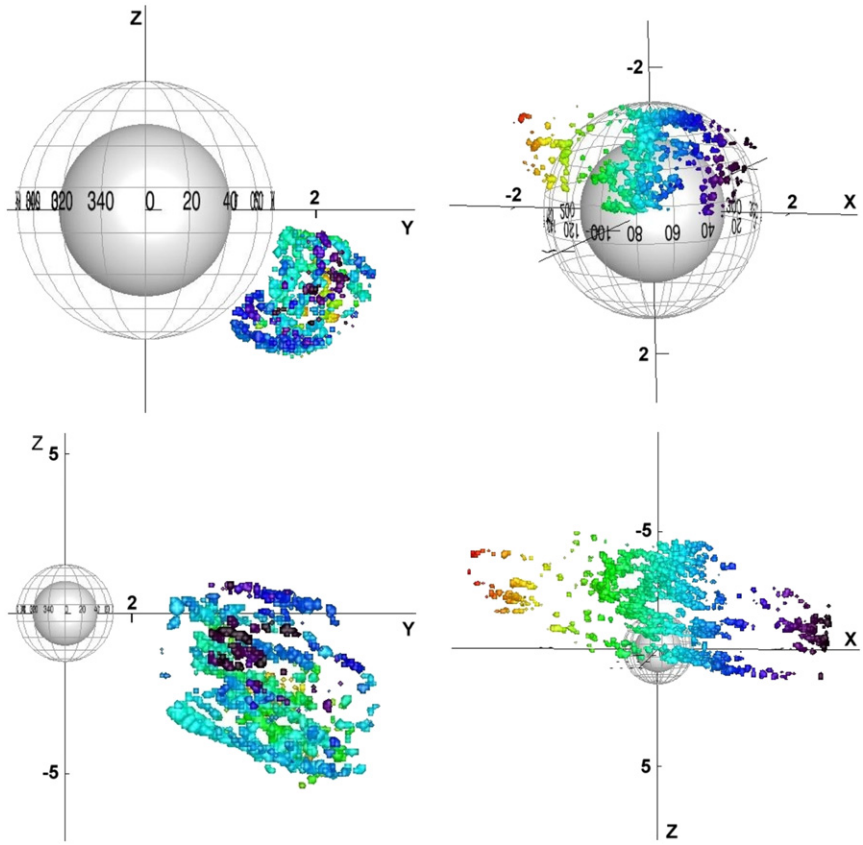

Fig. 2. LCT–TP reconstruction of the CME on 31 August 2007, COR1 data (upper panels) and COR2 data (lower panels). Left panels show the CME seen edge on and right panels represent the CME seen head on. The numbers on the sphere are the values of HEEQ longitudes. Note that the right panels represent the CME as seen from the Earth. The images on the right panels were inverted such that solar north is pointing downwards.

distribution centered on the mean, indicating CME width as function of time. Left panel of Fig. 4 shows the longitude as function of time. We see that initially, in COR1 FOV, the longitudinal width increases (up to the time of 21:25 UT), and then it maintains a constant value of approximative 34°. The longitudinal width of the CME observed by COR2 increases from 18° (at 22:52 UT, 31 August 2007) to 44° (at 01:22 UT, 1 September 2007) and then it maintains a constant width. The mean value of the longitude decreases from 73° to 67° in COR1 FOV, which may indicate a deflection from the radial propagation direction. The latitudinal width in COR1 FOV (middle panel of Fig. 4) shows an increase from 18° to around 32°. The latitudinal width remains constant (around 26°) in COR2 FOV. The CME propagates approximately at the same latitude (of around −23°) in the COR1 FOV and −18° in COR2 FOV.

Starting with 01:22 UT, when the mean height was around $6.88R_{\odot}$, it is observed that both latitudinal and longitudinal widths are constant, indicating a self-similar expansion of the CME. Both latitude and longitude mean values show a jump from COR1 to COR2 FOV. This may indicate a deflection from the radial propagation direction or it can be instrumental due to incorrect alignment or calibration of COR1 and COR2 instruments. This effect is not observed anymore above a height of around $6.9R_{\odot}$.

The mean height shows an increase and then a decrease for both COR1 and COR2 FOVs (Fig. 4, right panel). The decrease may be related to the fact that at later times, the front of the CME is not well visible in the coronagraph images and the core points have more weight over the CME structure.

The longitudinal extent ($Lon_{max} - Lon_{min}$) and the latitudinal extent ($Lat_{max} - Lat_{min}$) are shown in Table 1. Lon_{max} and Lon_{min} represent the maximum and the minimum values of the longitude of the reconstructed CME at a given time. The mean values for longitude and latitude extents in time are around $94° \pm 16°$ and $50° \pm 6°$, respectively. This is consistent with the widths of the CMEs, as derived from LASCO images: mean value of 85°, ranging from 30° to 180° (see Cremades and Bothmer, 2004). Note that the widths derived from LASCO are taken from statistics and they are projected plane-of-the-sky widths for structured CMEs only. In general, the latitude extent is smaller than the longitude extent (see Table 1), indicating an elliptical cone like structure (Cremades and Bothmer, 2005; Michaleck, 2006; Zhao, 2008) or a croissant structure (Chen, 1996; Thernisien et al., 2006, 2009).

4.2. Reconstruction constraints

The spread of the reconstructed correlation sources as shown in Fig. 2 should indicate the CME shape. We have to keep in mind, however, that the LCT method relies on statistical correlations and therefore may include quite some noise. In general, the reconstruction of the full 3D geometry of the CMEs from only two vantage directions is complicated by several factors: (1) the complexity of the CME morphology (as observed in coronagraphs, they can have bubble-like shapes, twisted shapes, etc.); (2) correct identification of the same feature in the two images; (3) optically thin CME plasma. A further constraint of the method (and white-light observations in general) is the line-of-sight integrated intensity, which restricts any extraction of information on the internal structure of the CME.

The LCT method itself has several undesired effects, such as (a) the technique attempts to find correlation maxima from noisy intensity data (low intensity or low signal-to-noise pixels) and (b) for a given window position in image A, correlation maxima

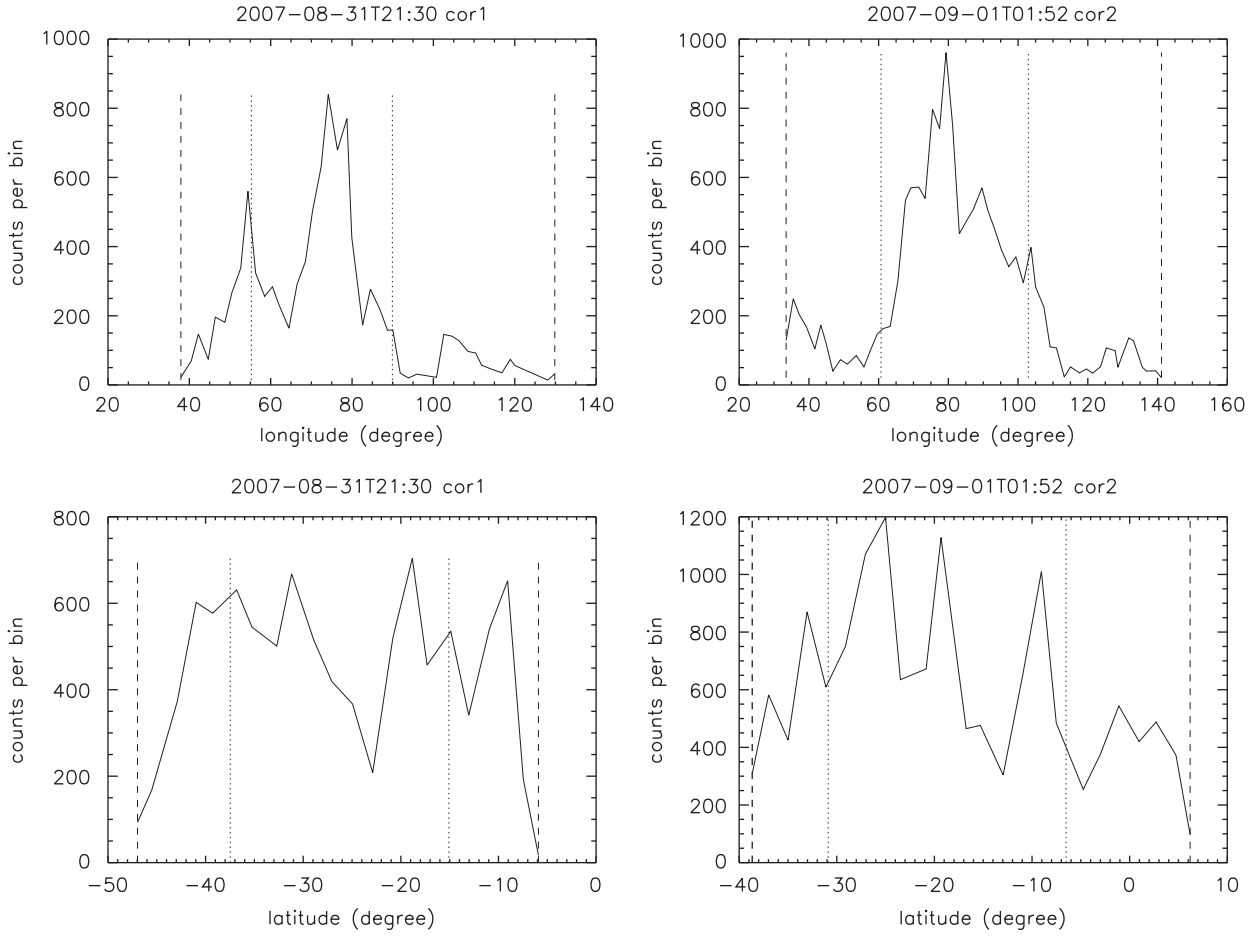

Fig. 3. Histogram of points for the reconstructed CME on 31 August 2007, 21:30 UT (left panels) and on 1 September 2007, 01:52 UT (right panels). The upper panels show the distribution over longitude and the lower panels show the distribution over latitude. The vertical dotted lines indicate the width and the vertical dashed lines indicate the extent of the CME as defined in the manuscript.

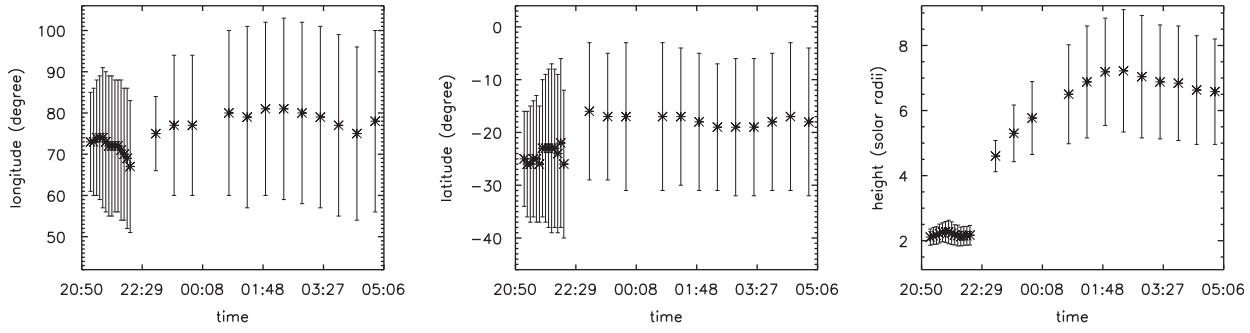

Fig. 4. Left panel: Mean value of longitudes $\pm$ one standard deviation (σ). Middle panel: Mean value of latitudes $\pm$ one standard deviation (σ). Right panel: Mean value of height $\pm$ one standard deviation (σ). The size of the error bar, from its top to its bottom, indicates the longitudinal (left panel) and latitudinal (middle panel) width of the CME.

may be found for more than one window position in image B. In the case of the CME on 31 August 2007, the main problem was the noise in the CME data, and in order to reduce it, we have chosen to threshold the image intensities by 120 DN (digital number) for COR1 and 4 DN for COR2. All the pixels below these values were ignored. These values usually corresponded to the faint features inside the ROI.

4.3. Application of LCT–TP method to a model data

The spread along *X*-direction should indicate the depth of the CME, if the correlation maxima are due to the same features in A and B images. As we have no means to check the real depth extension of this CME, we compare our results with those from the flux rope fit procedure described by Thernisien et al. (2006).

4.3.1. The model data

By applying the forward modeling to the CME observed by COR1 (at 21:30 UT) we obtain values for various parameters. The latitude (θ) and longitude (φ) of the main propagation direction are -19° and 63°, respectively; the tilt angle of the flux rope with respect to the solar equator (γ) is 65°; the outer shell height is $3.21R_\odot$, the ratio of minor torus radius to the distance from the Sun's center (κ) is 0.4 and the angular width (or the angle between the legs of a croissant-like CME: $2\cdot\alpha$) is 17° (see Mierla et al., 2009). Note, that flux tube fit

Table 1
Longitudinal extent ($Lon_{max}-Lon_{min}$) and latitudinal extent ($Lat_{max}-Lat_{min}$) of reconstructed points at different times.

Time (UT), COR1	Lon. extent (deg), COR1	Lat. extent (deg), COR1	Time (UT), COR2	Lon. extent (deg), COR2	Lat. extent (deg), COR2
21:05	85	38	22:52	54	46
21:10	82	37	23:22	96	49
21:15	80	41	23:52	109	52
21:20	79	50	00:52	114	51
21:25	91	41	01:22	111	51
21:30	92	41	01:52	107	47
21:35	97	57	02:22	111	49
21:40	87	55	02:52	111	50
21:45	81	55	03:22	110	50
21:50	84	60	03:52	112	49
21:55	82	57	04:22	111	51
22:00	82	55	04:52	112	56
22:05	79	57			
22:10	82	57			

is primarily sensitive to the CME front visible in the images and also does not provide a reliable estimate of the longitude extent of the CME. In the case of this CME, the method gave robust estimates for the CME minor (=flux rope cross-section radius) radius and its latitude. The CME mean longitude is provided from the knowledge of the source region on the solar surface. The aspect ratio is less certain, due to the orientation of the CME with respect to the observation direction.

To calculate the longitude ($2\cdot\varepsilon$) and latitude ($2\cdot\omega$) extents we used the following equations (see Rodriguez et al., 2009):

$$\omega = \arcsin(\sin\alpha\cdot\sin\gamma)+\beta \quad (1)$$

$$\varepsilon = \arcsin\left(\frac{\sin\alpha\cdot\cos\gamma}{\cos\omega}\right)+\beta \quad (2)$$

where $\beta=\arctan(\kappa)$ represents the width of the legs cross-section of the flux rope like model (see Thernisien et al., 2006), ω is the angular half width of the CME perpendicular to the solar equator, and ε is the corresponding half width parallel to the solar equator (or the half longitudinal extension of the CME). The extent in HEEQ coordinate system will be then $2\cdot\varepsilon$ in longitude and $2\cdot\omega$ in latitude. The parameters of the forward modeling yield a longitude extent of approximately 52° and a latitude extent of approximately 58° for the CME observed by COR1 at 21:30 UT. We have performed an error analysis of these quantities by using the errors of the model parameters as derived by Thernisien et al. (2009). The errors for longitude and latitude reported by Thernisien et al. (2009) are not constant and range from 1.5° to 16.6° with a mean value of 4.3° for the longitude and from 0.9° to 3.7° with a mean value of 1.8° for the latitude. By including the above values of the errors in our formula we obtain that the mean deviation ranges from 6° to 42°, with an average value of 16° for the longitudinal extent and from 8° to 64°, with an average value of 24° for the latitudinal extent.

Note that the errors may be small or large depending on the uncertainties in deriving model parameters.

4.3.2. Application of the LCT–TP method to model data: results

We applied the LCT–TP method to synthetic total brightness images (Mierla et al., 2009), derived from the model CME described in Section 4.3.1, whose longitudinal and latitudinal extents are known, i.e. 52° and 58°, respectively. We obtained a longitudinal extent ($Long_{max}-Long_{min}$) of around 102° and a latitudinal extent of around 61°. As we mentioned in Section 4.1, our analysis is based on a statistical approach, therefore quite large scatter is expected. The method is sensitive to outliers and extreme points and still misses robustness against these points. The nature of the distribution of points along both axis is also unknown and could lead to this unreliable estimation (note that the derived longitudinal extent is twice as compared to the real value). The latitudinal extent matches pretty well.

The mean value derived for the longitude is $60^\circ\pm17^\circ$ and for the latitude is $-20^\circ\pm18^\circ$ for the model CME. The mean values derived by applying the method to the real CME at 21:30 UT are: $73^\circ\pm17^\circ$ for longitude and $-26^\circ\pm11^\circ$ for latitude. We see that the values overlap if the errors are taken into account.

5. Summary

The LCT–TP results show some scatter in the direction parallel to the line-of-sight. The spread should indicate the depth of the CME, if the correlation maxima are due to identical plasma fluctuations inside the CME. However, as it is a statistical approach some noise and scatter is expected. In order to check our results, we apply the LCT–TP method to a model CME whose latitudinal and longitudinal extents are known: 58° and 52° respectively. We estimated a longitudinal width of 102°, almost twice that of the real value. The estimated latitudinal extent was 61°, very similar to the real value. This indicates that a large scatter is expected when deriving the depth information. The errors in the estimation of depth, that is the distance from the plane of sky to an object seen by a virtual observer half way between the two spacecraft, depend on the separation angle between the two spacecraft as: $ds/\sin(\gamma/2)$, where ds is the pointing error (or the error in choosing similar features on two STEREO images) and γ is the base angle between STEREO spacecraft (see e.g. Inhester, 2006). This implies that the error should decrease with increasing separation angle, but the identification of similar features in two images becomes difficult when the separation is large. For our event, γ had a value of approximately 28°, and a pointing error of 1 pixel will yield a longitude error of 1° for a feature situated at $2R_\odot$ (COR1) and $7R_\odot$ (COR2) (see Mierla et al., 2009).

By applying the LCT–TP method to the CME on 31 August 2007, at different instants, we obtained longitudinal extents of approximately $94^\circ\pm16^\circ$ and latitudinal extents of approximately $50^\circ\pm6^\circ$. In general, the latitudinal extent is smaller than the longitudinal extent, indicating an elliptical cone like structure or a flux rope like structure of the CME (see e.g. Cremades and Bothmer, 2005; Thernisien et al., 2006). As the LCT–TP method is a statistical approach we define the widths of the distribution as $2\cdot\sigma$ and analyze their behavior in time. They vary from 18° to 44° for the longitude and from 18° to 32° for the latitude. From a height above $6.9R_\odot$, a self-similar expansion is observed.

In general the method shows a large scatter in longitudinal extent, and in order to validate this method more CMEs have to be reconstructed using this technique.

Acknowledgements

The authors thank the anonymous referees for useful comments that have greatly improved the manuscript. M.M. would like to thank C. Marque for productive discussions. We acknowledge the STEREO/SECCHI and SOHO/LASCO consortia for providing the data. The SECCHI data used here were produced by an International Consortium of the Naval Research Laboratory (USA), Lockheed Martin Solar and Astrophysics Lab (USA), NASA Goddard Space Flight Center (USA), Rutherford Appleton Laboratory (UK), University of Birmingham (UK), Max-Planck Institute for Solar System Research (Germany), Centre Spatiale de Liège (Belgium), Institut d'Optique Théorique et Appliquée (France), Institut d'Astrophysique Spatiale (France). The LASCO data used here were produced by an

International Consortium of the Naval Research Laboratory (USA), the Laboratoire d'Astrophysique de Marseille (France, the former Laboratoire d'Astronomie Spatiale), the Max-Planck Institute for Solar System Research (Germany), and the School of Physics and Astronomy, University of Birmingham (UK). SoHO is a project of joint collaboration by ESA and NASA.

References

Antunes, A., Thernisien, A., Yahil, A., 2009. Hybrid reconstruction to derive 3D height-time evolution for coronal mass ejections. Sol. Phys. 259, 199–212.
Billings, D.E., 1966. A guide to the Solar Corona. Academic Press, NY, London.
Chen, J., 1996. Theory of prominence eruption and propagation: interplanetary consequences. J. Geophys. Res. 101, 27499–27520.
Cremades, H., Bothmer, V., 2004. On the three-dimensional congiguration of coronal mass ejections. Astron. Astrophys. 422, 307–322.
Cremades, H., Bothmer, V., 2005. Geometrical properties of coronal mass ejections. In: Dere, K., Wang, J., Yan, Y. (Eds.), IAU Symposium Proceedings of the International Astronomical Union 226, Cambridge University Press, pp. 48–54.
Dere, K.P., Wang, D., Howard, R., 2005. Three-dimensional structure of coronal mass ejections from LASCO polarization measurements. Astrophys. J. 620, L119–L122.
Gopalswamy, N., Yashiro, S., Akiyama, 2007. Geoeffectiveness of halo coronal mass ejections. J. Geophys. Res. 112, A06112. doi:10.1029/2006JA012149.
Howard, T.A., Three-dimensional reconstruction of coronal mass ejections using heliospheric imager data. J. Atmos. Sol. Terr. Phys., this issue.
Howard, T.A., Tappin, S.J., 2009. Interplanetary coronal mass ejections observed in the heliosphere: 1. Review of theory, SSRv 147, 31–54.
Illing, R.M.E., Hundhausen, A.J., 1986. Disruption of a coronal streamer by an eruptive prominence and coronal mass ejection. J. Geophys. Res. 91, 10951–10960.
Inhester, B., 2006. Stereoscopy basics for the STEREO mission, astro-ph/0612649.
Jackson, B.V., Hicka, P.P., Buffington, A., Bisi, M.M., Clover, J.M., Tokumaru, M., Kojima, M., Fujiki, K. Three-dimensional reconstruction of heliospheric structure using iterative tomography: a review. J. Atmos. Sol. Terr. Phys., this issue.
Michaleck, G., 2006. An asymmetric cone model for halo coronal mass ejections. Sol. Phys. 237, 101–118.
Mierla, M., Inhester, B., Marque, C., Rodriguez, L., Gissot, S., Zhukov, A., Berghmans, D., Davila, J., 2009. On 3D reconstruction of coronal mass ejections: I method description and application to SECCHI-COR data. Sol. Phys. 259, 123–141.
Mierla, M., Inhester, B., Antunes, A., Boursier, Y., Byrne, J.P., Colaninno, R., Davila, J., deKoning, C.A., Gallager, P.T., Gissot, S., et al., 2010. On the 3D reconstruction of coronal mass ejections using coronagraph data. Ann. Geophys. 28, 203–211.
Moran, T.G., Davila, J.M., 2004. Three-dimensional polarimetric imaging of coronal mass ejections. Science 305, 66–71.
Moran, T.G., Davila, J.M., Thompson, W.T., 2010. Three-dimensional polarimetric coronal mass ejection localization tested through triangulation. Astrophys. J. 712, 453–458.
Rodriguez, L., Zhukov, A.N., West, M., Kilpua, E., Mierla, M., Linking CMEs observed by STEREO with their interplanetary counterparts. In: Solar Wind 12, Saint-Malo, France, 21–26 June 2009 (poster).
Rouillard, A. Relating white light and in situ observations of coronal mass ejections: a review. J. Atmos. Sol. Terr. Phys., this issue.
Srivastava, N., Venkatakrishnan, P., 2004. Solar and interplanetary sources of major geomagnetic storms during 1996–2002. J. Geophys. Res. 109, A10103. doi:10.1029/2003JA010175.
Thernisien, A.F.R., Howard, R.A., Vourlidas, A., 2006. Modeling of flux rope coronal mass ejections. Astrophys. J. 652, 763–773.
Thernisien, A., Vourlidas, A., Howard, R.A., 2009. Forward modelling of coronal mass ejections using STEREO-SECCHI data. Sol. Phys. 256, 111–130.
Vourlidas, A., Howard, R.A., 2006. The proper treatment of coronal mass ejection brightness: a new methodology and implications for observations. ApJ 642, 1216–1221.
Wood, B.E., Howard, R.A., Thernisien, A., Plunkett, S.P., Socker, D.G., 2009. Reconstructing the 3D Morphology of the 17 May 2008 CME. Sol. Phys. 259, 163–178.
Zhao, X.P., 2008. Inversion solutions of the elliptic cone model for disk frontside full halo coronal mass ejections. J. Geophys. Res. 113, A02101.